

RESEARCH ARTICLE

10.1002/2016JC011797

Key Points:

- A peak at ~761 nm from reflectance spectra of natural waters has been treated as measurement artifacts in the past
- We demonstrate that the peak is due to chlorophyll *a* fluorescence through the fill-in effects on the Telluric lines
- The height of fluorescence peak (*FLH*) at 761 nm has stronger correlation with *Chl a* concentration than *FLH*(~685)

Correspondence to:

Y. Lu,
luyc@nju.edu.cn;
L. Li,
lil032@ucsd.edu
who contributed equally

Citation:

Lu, Y., L. Li, C. Hu, L. Li, M. Zhang, S. Sun, and C. Lv (2016), Sunlight induced chlorophyll fluorescence in the near-infrared spectral region in natural waters: Interpretation of the narrow reflectance peak around 761 nm, *J. Geophys. Res. Oceans*, 121, 5017–5029, doi:10.1002/2016JC011797.

Received 13 MAR 2016

Accepted 13 JUN 2016

Accepted article online 16 JUN 2016

Published online 24 JUL 2016

Sunlight induced chlorophyll fluorescence in the near-infrared spectral region in natural waters: Interpretation of the narrow reflectance peak around 761 nm

Yingcheng Lu^{1,2,3}, Linhai Li⁴, Chuanmin Hu³, Lin Li⁵, Minwei Zhang³, Shaojie Sun³, and Chunguang Lv¹

¹Jiangsu Provincial Key Laboratory of Geographic Information Science and Technology, International Institute for Earth System Science, Nanjing University, Nanjing, China, ²State Key Laboratory of Satellite Ocean Environment Dynamics, Second Institute of Oceanography, State Oceanic Administration, Hangzhou, China, ³College of Marine Science, University of South Florida, St. Petersburg, Florida, USA, ⁴Marine Physical Laboratory, Scripps Institution of Oceanography, University of California San Diego, La Jolla, California, USA, ⁵Department of Earth Sciences, Indiana University-Purdue University Indianapolis, Indianapolis, Indiana, USA

Abstract Sunlight induced chlorophyll *a* fluorescence (SICF) can be used as a probe to estimate chlorophyll *a* concentrations (*Chl*) and infer phytoplankton physiology. SICF at ~685 nm has been widely applied to studies of natural waters. SICF around 740 nm has been demonstrated to cause a narrow reflectance peak at ~761 nm in the reflectance spectra of terrestrial vegetation. This narrow peak has also been observed in the reflectance spectra of natural waters, but its mechanism and applications have not yet been investigated and it has often been treated as measurement artifacts. In this study, we aimed to interpret this reflectance peak at ~761 nm and discuss its potential applications for remote monitoring of natural waters. A derivative analysis of the spectral reflectance suggests that the 761 nm peak is due to SICF. It was also found that the fluorescence line height (*FLH*) at 761 nm significantly and linearly correlates with *Chl*. *FLH*(761 nm) showed a tighter relationship with *Chl* than the relationship between *FLH*(~685 nm) and *Chl* mainly due to weaker perturbations by nonalgal materials around 761 nm. While it is not conclusive, a combination of *FLH*(761 nm) and *FLH*(~685 nm) might have some potentials to discriminate cyanobacteria from other phytoplankton due to their different fluorescence responses at the two wavelengths. It was further found that reflectance spectra with a 5 nm spectral resolution are adequate to capture the spectral SICF feature at ~761 nm. These preliminary results suggest that *FLH*(761 nm) need to be explored more for future applications in optically complex coastal and inland waters.

1. Introduction

Sunlight induced chlorophyll fluorescence (SICF) is a probe for inferring the status of photosynthesis. It has a sharp peak at ~685 nm and a broad shoulder at ~740 nm [e.g., Krause and Weis, 1991; Meroni and Colombo, 2006; Zarco-Tejada et al., 2009]. The detected SICF signals from marine phytoplankton and terrestrial vegetation have been widely used to estimate chlorophyll *a* concentrations (*Chl*) or detect phytoplankton blooms [e.g., Tyler and Smith, 1970; Gordon, 1979; Gitelson, 1992; Hu et al., 2005; Meroni et al., 2009]. The SICF at ~685 nm has been measured, verified, and applied to natural waters in numerous studies [e.g., Gordon, 1974; Neville and Gower, 1977; Gordon, 1979]. However, the SICF signal at ~740 nm has not been investigated for natural waters, while the SICF at ~740 nm has been commonly used in the remote sensing of terrestrial vegetation [e.g., Krause and Weis, 1991; Meroni and Colombo, 2006; Zarco-Tejada et al., 2009]. The SICF at ~740 nm causes a noticeable peak at ~761 nm in the reflectance spectra of terrestrial vegetation, which is due to the fill-in effects of Telluric lines by SICF [Meroni et al., 2009; Zarco-Tejada et al., 2009; Meroni and Colombo, 2006]. However, although a number of published works retrieved fluorescence from terrestrial plants (see above cited references), the use of a 761 nm band for the aquatic phytoplankton has not been reported in the literature because it has been commonly treated as measurements artifacts.

Telluric lines, the narrow troughs in the terrestrial solar irradiance spectrum, are caused by the absorption of gases in the Earth's atmosphere [Meroni et al., 2009]. The terrestrial solar irradiance within the range of

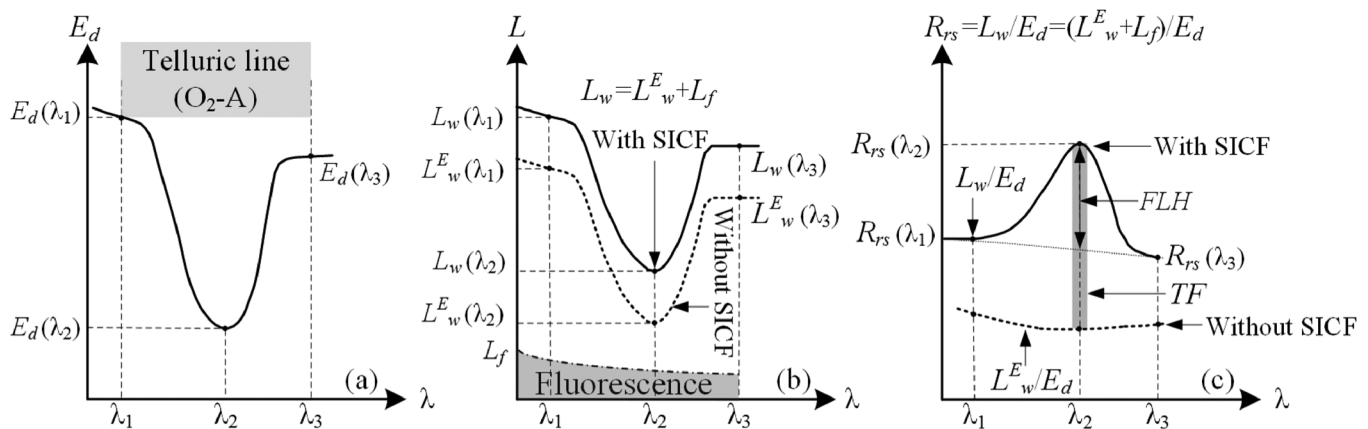


Figure 1. Schematic graph showing the detection of SICF within Telluric lines at ~ 761 nm. (a) Downwelling solar irradiance (E_d) around the Telluric line due to oxygen absorption (O_2 -A); (b) water-leaving radiances (L_w) including radiance due to elastic processes L_w^E , radiance due to fluorescence L_f , and the total radiance ($L_w = L_w^E + L_f$); (c) remote sensing reflectance R_{rs} with and without the contribution of fluorescence. Refer to the text for the definition of the symbols and acronyms in this figure. This figure was inspired by Moya *et al.* [2004, Figure 2] in which downwelling irradiance and upwelling radiance were also shown in relative units.

Telluric lines is dramatically reduced compared to those at adjacent spectral ranges outside Telluric lines. At a wavelength of ~ 761 nm, the main Telluric characteristics are caused by the absorption of oxygen (O_2 -A, centered at 761.035 nm) in the Earth's atmosphere [Meroni *et al.*, 2009; Damm *et al.*, 2011].

Figure 1a shows the shape of illustrative terrestrial downwelling solar irradiance ($E_d(\lambda)$; hereafter, the dependence on wavelength λ is dropped for simplicity unless it causes ambiguity) with 3 nm spectral resolution around the O_2 -A band based on MODTRAN 5.3 simulations for a 1976 U.S standard atmosphere and maritime aerosols with 23 km visibility. The affecting wavelengths range from λ_1 (~ 758 nm) to λ_3 (~ 771 nm), with the center of the trough at λ_2 (~ 761 nm), and the corresponding downwelling solar irradiances are $E_d(\lambda_1)$, $E_d(\lambda_3)$, and $E_d(\lambda_2)$, respectively. When the sunlight enters and interacts with a water medium, the radiance that leaves the water, L_w , includes the contribution of an elastic component, L_w^E , and inelastic components such as fluorescence, L_f (Figure 1b). L_w^E is the product of E_d in Figure 1a and $0.33 \times b_b/(a + b_b)$ [Gordon *et al.*, 1988] where b_b and a are total backscattering and absorption coefficients of moderately turbid waters. The relative shape of L_f was taken from Meroni and Colombo [2006]. The corresponding remote sensing reflectance (R_{rs} , sr^{-1}) spectra with and without L_f are shown in Figure 1c. The example in Figure 1 only shows the relative shapes of the displayed parameters, which do not represent any specific case. It implies that the spectral peak around O_2 -A bands may not be observed in the R_{rs} spectrum without contribution of L_f , while a noticeable peak can be found when chlorophyll fluorescence was included. The same principle of fill-in of O_2 absorption lines around 689 nm has actually been used to measure solar-stimulated fluorescence around 685 nm in water [Hu and Voss, 1998]. The total SICF signal around the peak centered at 761 nm is defined as the total fluorescence line height (TF, see Figure 1c) which cannot be retrieved from in situ reflectance spectra. However, fluorescence line height (FLH, see Figure 1c) can be derived from the R_{rs} spectrum and is proportional to TF (see section 2.3.2 for details). FLH does not represent the radiance produced by SICF but is an index that shows the relative strength of the SICF.

As explained above, the SICF signal at ~ 740 nm can result in a spectral reflectance peak at ~ 761 nm where the Telluric lines caused by O_2 absorption are found. Such a phenomenon has been investigated in remote sensing of terrestrial vegetation [Zarco-Tejada *et al.*, 2009] but not in water applications. In this study, we aimed to demonstrate that SICF can also cause a narrow peak at ~ 761 nm in the spectral reflectance of natural waters. The correlation analysis between the first-order derivative of R_{rs} at ~ 761 nm as well as the relationship between FLH(761 nm) and *Chl* will be discussed below to support our arguments. The work is not to develop a *Chl* retrieval algorithm, but to demonstrate that the reflectance peak at ~ 761 nm from natural waters may not be a measurement artifact but a result of solar-stimulated fluorescence. We hope this work stimulates further investigations by the ocean color community into the potential causes and applications of the narrow reflectance peak at ~ 761 nm, especially for coastal and inland waters where the optical signal remains strong to be accurately detected in this spectral region.

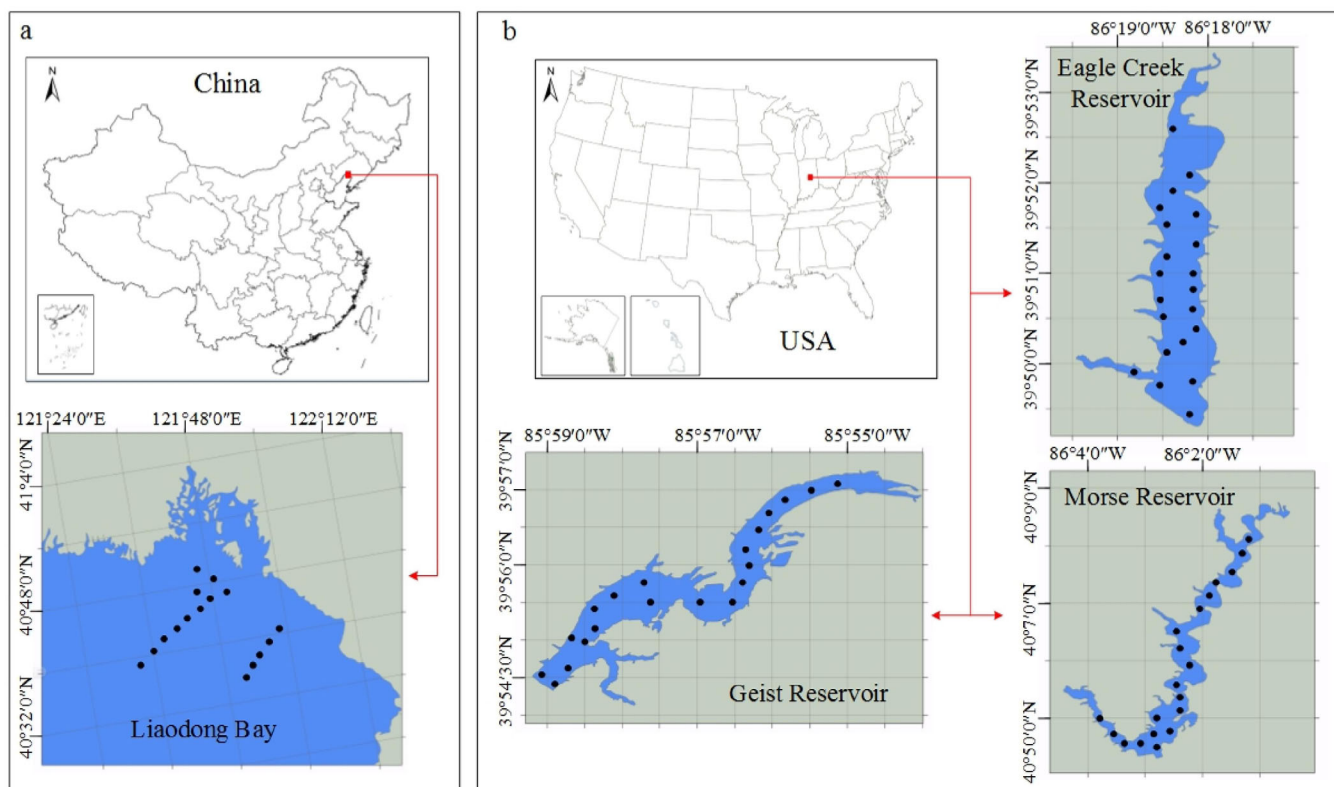


Figure 2. The study areas. (a) Liaodong Bay, China; (b) three Indiana reservoirs (Eagle Creek Reservoir, Geist Reservoir, and Morse Reservoir), USA. The black dots represent the sample sites during multiple field campaigns.

2. Materials and Methods

2.1. Study Area

The study areas included Liaodong Bay in China and three reservoirs in Indiana, USA (Figure 2). Liaodong Bay is located in the northern coastal region of Bohai Sea, the largest inland sea of China. The average depth is approximately 18 m. The water surface temperature is approximately 24°C–25°C. During the summer, the wind speed is 4–5 m/s. Two inland rivers, i.e., the Shuangtaizi River and Liaohe River, flow into Liaodong Bay in this area. Therefore, the ocean color is complex with a high suspended particulate material (mostly nonalgal particles) concentration (*SPM*), which is a main characteristic of this study area (i.e., *SPM* is generally higher than 100 g/m³). The three reservoirs in Indiana are the Eagle Creek Reservoir (ECR, 39°51'N, 86°18.3'W), Geist Reservoir (GR, 39°55'N, 85°56.7'W), and Morse Reservoir (MR, 40°6.4'N, 86°2.3'W). These reservoirs have similar depths (3.2–4.7 m), surface areas (5–7.5 km²), and volumes (21–28 × 10⁶ m³). They all face a serious eutrophication problem that leads to frequent toxic cyanobacterial blooms. As a result, the *SPM* contains a large contribution of phytoplankton when the *SPM* is relatively low; e.g., typically less than 30 g/m³. More information about the three reservoirs can be found in *Li et al.* [2013, 2015].

2.2. In Situ Measurements

2.2.1. Hyperspectral Reflectance

In Liaodong Bay (Figure 2a), an ASD spectroradiometer (Analytical Spectral Devices, Inc., Boulder, CO, USA) system with a single radiometer and a 100% reflecting white panel was used to determine reflectance spectra. In the visible and near-infrared (VNIR) wavelengths of detection (350–1050 nm), the spectral resolution is 3 nm with 1.4 nm sampling intervals and 0.5 nm wavelength accuracy, and the data were resampled to 1 nm spectral interval. The upwelling radiance of the water surface, L_t , was first determined by pointing the radiometer towards the water surface, followed by the determination of downwelling irradiance, E_d , on a Spectralon panel (Labsphere Inc., North Sutton, NH) using the same radiometer. Two field campaigns were

conducted on 17–18 September 2006 and 22–23 August 2007. The local observation time was from 10:00 A.M. to 14:00 P.M. We collected, in total, 32 valid reflectance spectra, where the reflectance (R) was calculated as

$$R = \frac{L_t}{E_d} = \frac{L_w + L_s}{E_d}, \tag{1}$$

where L_w is the water leaving-radiance (including the contribution of L_f), and L_s is the Fresnel reflected radiance by the water surface. The measured R is not a conventional definition of remote sensing reflectance ($R_{rs} = L_w/E_d$) due to the extra term L_s in the numerator. The impact of L_s on data interpretation will be discussed in section 4.1.

In three Indiana reservoirs (Figure 2b), an Ocean Optics USB4000 system (Ocean Optics, Inc., Dunedin, FL, USA) with dual radiometers was used to measure R_{rs} from April to October in 2010. The two radiometers were connected to different Ocean Optics consoles. The measurements by the two radiometers were resampled to the same spectral wavelengths before computing remote sensing reflectance. The reflectance was measured by following the procedure described in *Gitelson et al.* [2007]. Mounted on a 2 m pole, radiometer #1 was pointed upward to measure the real-time incident E_d through a cosine collector, and simultaneously radiometer #2 was dipped ~2 cm below the water surface via a 2 m pole to measure the below-surface upwelling radiance $L_u(0^-)$ at the nadir. For every few stations or under changing sky conditions, the instrument was manually calibrated by measuring the L_{cal} on a Spectralon panel with reflectance ρ and the corresponding real-time downwelling irradiance E_{dcal} in air, and this calibration was automatically used for subsequent measurements until a new calibration was performed. The field measurements were later processed to remote sensing reflectance using the software provided by the manufacturer:

$$R_{rs} = \frac{L_w}{E_d} = \frac{t}{n^2} \frac{L_u(0^-)}{E_d} \frac{\rho E_{dcal}}{\pi L_{cal}} F, \tag{2}$$

where F is the spectral immersion factor, t is the transmittance of the water-air interface, and n is the refractive index of water medium. t/n^2 is generally a constant; i.e., 0.54 [Mobley, 1999]. The measured spectra of R and R_{rs} are shown in Figure 3.

2.2.2. Chlorophyll a and Suspended Particulate Matter Concentrations

Concurrent with the reflectance measurements, water samples were collected and sent to the laboratory to determine the *Chl* (mg/m^3) and *SPM* (g/m^3). *Chl* was measured using the spectrophotometric method [Ritchie, 2008] and the *SPM* concentration was determined using the gravimetric weighing method for both Liaodong Bay and the Indiana reservoirs. The statistics of the measured *Chl* and *SPM* are shown in Table 1.

2.3. Methods

2.3.1. Spectral Derivative

The spectral derivative (*SD*) is defined in equation (3):

$$SD(\lambda_i) = \frac{R_{rs}(\lambda_{i+1}) - R_{rs}(\lambda_{i-1})}{2\Delta\lambda}, \tag{3}$$

where R_{rs} can also be replaced by R , and $\Delta\lambda$ is the spectral resolution of the reflectance spectra (1 nm for our data set after resampling). *SD* is used to eliminate the impact of a linear background on the R_{rs} spectrum and detect the change in positions of reflectance peaks [Lee et al., 2007, and references therein]. Therefore, the correlation between *SD* of R_{rs} and *Chl* can help to identify the spectral reflectance peaks caused by chlorophyll, e.g., SICF. In this study, *SD* was also used to determine the wavelengths λ_1 , λ_2 , and λ_3 that were used to compute the *FLH* in section 2.3.2.

2.3.2. Fluorescence Line Height

As shown in Figure 1c, the *TF* on the R_{rs} around λ_2 should be

$$TF(\lambda_2) = \frac{L_w^E(\lambda_2) + L_f(\lambda_2)}{E_d(\lambda_2)} - \frac{L_w^E(\lambda_2)}{E_d(\lambda_2)} = \frac{L_f(\lambda_2)}{E_d(\lambda_2)}, \tag{4}$$

and the *FLH*(λ_2) is

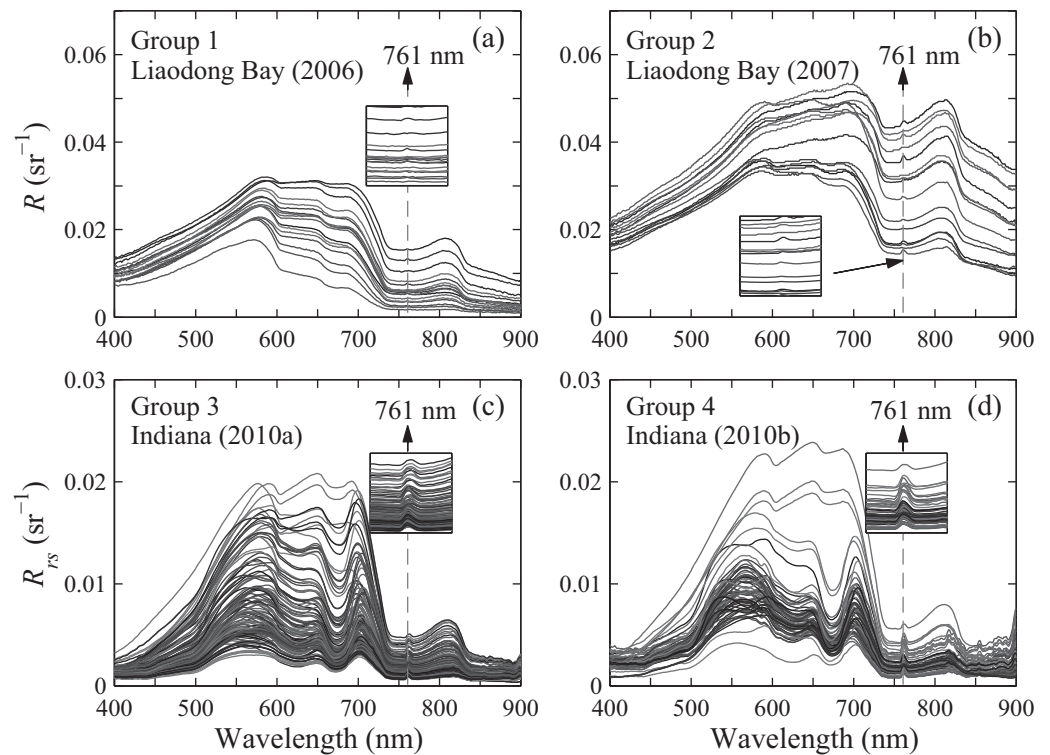


Figure 3. Reflectance (R , sr^{-1} , equation (1)) spectra of Liaodong Bay (a) group 1 in 2006 and (b) group 2 in 2007, and remote sensing reflectance (R_{rs} , sr^{-1} , equation (2)) spectra of Indiana reservoirs (c) group 3 and (d) group 4. The inset in each plot shows the reflectance spectra around 761 nm. The data set is divided into four groups due to different concentrations of suspended particulate matter and phytoplankton composition. The detailed reasons to classify the spectra into four groups can be found in section 4.2.

$$FLH(\lambda_2) = R_{rs}(\lambda_2) - \left[\frac{\lambda_3 - \lambda_2}{\lambda_3 - \lambda_1} (R_{rs}(\lambda_1) - R_{rs}(\lambda_3)) + R_{rs}(\lambda_3) \right]. \quad (5)$$

Within the spectral range around λ_2 but outside the $\text{O}_2\text{-A}$ band, $R_{rs}(\lambda_1) \approx R_{rs}(\lambda_3)$. Therefore,

$$FLH(\lambda_2) \approx R_{rs}(\lambda_2) - R_{rs}(\lambda_3) = \frac{L_w^E(\lambda_2) + L_f(\lambda_2)}{E_d(\lambda_2)} - \frac{L_w^E(\lambda_3) + L_f(\lambda_3)}{E_d(\lambda_3)}. \quad (6)$$

Assuming the wavelength dependency of L_f is relatively weak at ~ 761 nm (less than 10% change between 755 and 771 nm according to Meroni and Colombo [2006]) and applying $L_w^E(\lambda_2)/E_d(\lambda_2) \approx L_w^E(\lambda_3)/E_d(\lambda_3)$ (see Figure 1c) in equation (6) leads to:

$$FLH(\lambda_2) \approx (1 - T_a) \frac{L_f(\lambda_2)}{E_d(\lambda_2)} = (1 - T_a) \times TF(\lambda_2), \quad (7)$$

where $T_a = E_d(\lambda_2)/E_d(\lambda_3)$. Within the Telluric lines due to $\text{O}_2\text{-A}$, T_a generally ranges from 0.2 to 0.5 for different atmospheres and solar angles; however, it should be relatively stable across a small region (with similar solar angle and atmosphere), so changes in $FLH(\lambda_2)$ can be interpreted as changes in the fluorescence

Table 1. The Statistics of *Chl* and *SPM* for Each Group Shown in Figure 3

	<i>Chl</i> (mg/m^3)				<i>SPM</i> (g/m^3)			
	Min.	Max.	Avg.	Std.	Min.	Max.	Avg.	Std.
Group 1	2.39	16.52	8.60	4.08	87	315	188.82	59.38
Group 2	0.88	13.42	4.89	3.20	194	941	530.60	188.26
Group 3	1.85	129.39	53.33	29.98	5.17	36.17	15.32	6.10
Group 4 ^a	19.84	104.96	41.07	17.74	5.83	18.33	9.77	2.66

^aThe highest *SPM* for group 4, 81.17 g m^{-3} , was excluded in the statistics.

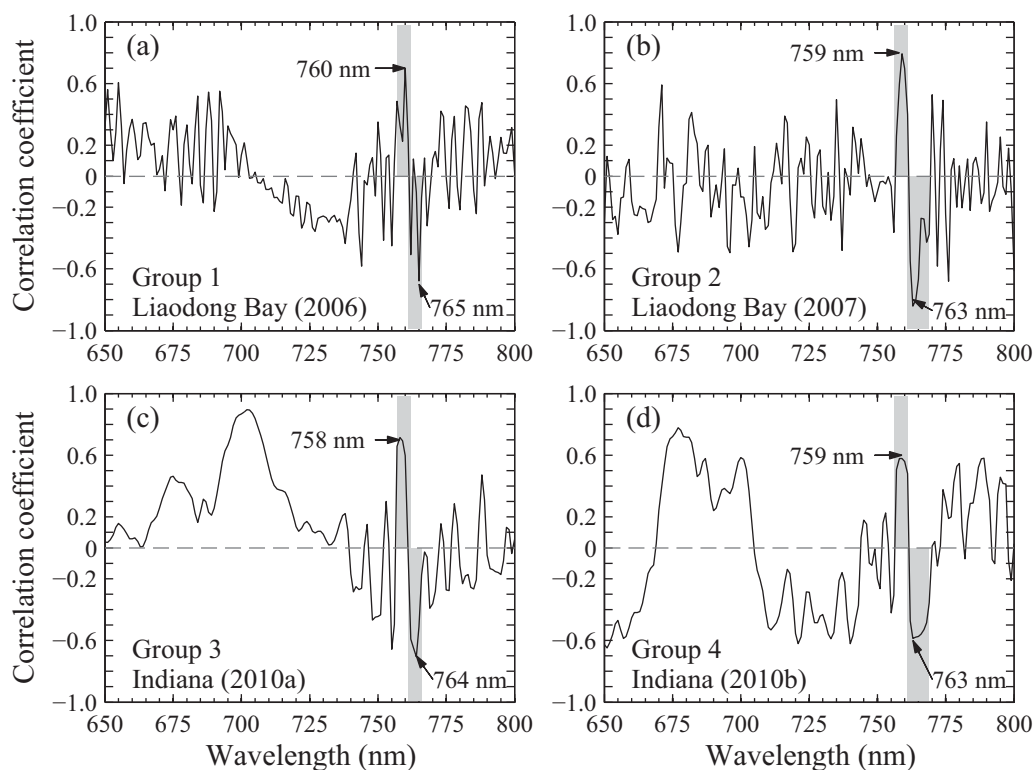


Figure 4. Correlation coefficients between the first-order spectral derivative of R or R_{rs} and Chl corresponding to the four groups shown in Figure 3.

signal. In other words, the $FLH(\lambda_2)$ for a particular image of a small region is proportional to the total SICF signal around λ_2 and could therefore possibly be used to infer biomass or chlorophyll a concentrations with cautions (see sections 4.2 and 4.3 for more detail).

3. Results

3.1. Spectral Derivative (SD) Analysis

The core idea of SD analysis is to use a first-order differential equation to eliminate the impact of a linear background on the R_{rs} spectrum and identify any spectral peaks that may be caused by SICF. Figure 4 shows the correlation coefficients between the SD and Chl in the spectral range of 650–800 nm.

Within the wavelength range around Telluric lines by O_2 -A, SD and Chl were significantly correlated at two wavelengths, which are located on the left and right side of the spectral peak at 761 nm. This suggests that both the increase in reflectance before the spectral peak of 761 nm and the decrease in reflectance after the spectral peak can be attributed to chlorophyll, which implies that the spectral peak at ~ 761 nm may be caused by SICF. Depending on the group of reflectance spectra, the wavelengths with the best correlation varied from 758 to 760 nm on the left side of the peak and from 763 to 765 nm on the right side of the peak.

3.2. Relationship Between FLH and Chl

To concurrently take account of the effects of Telluric lines due to O_2 -A absorption band located at 758.725–770.416 nm [Damm *et al.*, 2011] and the best sensitive bands (758–760 and 763–765 nm) from SD analysis (Figure 4a), λ_1 , λ_2 , and λ_3 were set as 755, 761, and 771 nm with a bandwidth of 1 nm and $FLH(761 \text{ nm})$ was calculated accordingly using equation (5). Figures 5a and 5b show the statistical relationship between $FLH(761 \text{ nm})$ and Chl in Liaodong Bay, corresponding to data collected in 2006 and 2007, respectively. The determination coefficients (r^2) between $FLH(761 \text{ nm})$ and Chl for 2006 and 2007 were 0.536 and 0.677, respectively, and the p values were both less than 0.05. Figures 5c and 5d show the

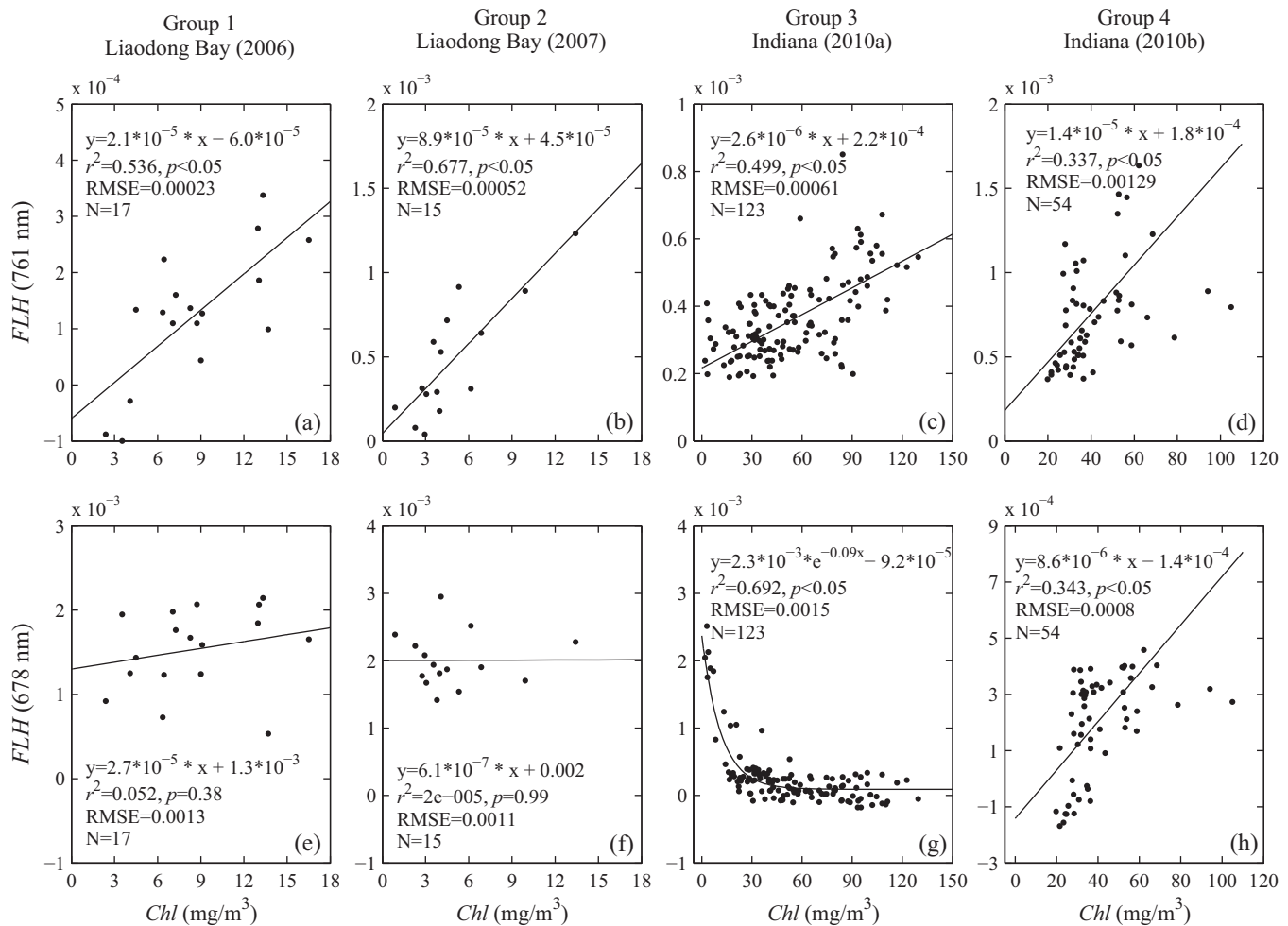


Figure 5. Relationships between (a–d) *FLH* (761 nm) and *Chl* as well as (e–h) *FLH* (678 nm) and *Chl* for the same four groups in Figures 3 and 4. Note: a few obvious outliers in Figures 5c and 5d were excluded from regression and the same stations were also excluded from regression analysis in Figures 5g and 5h, respectively.

relationships between *FLH*(761 nm) and *Chl* for an additional two groups of data collected from the three Indiana reservoirs, with the r^2 being 0.499 and 0.337, respectively and p values less than 0.05. These results indicate that a significant correlation between *FLH*(761 nm) and *Chl* exists for various limnological conditions at different study sites. In contrast, if the 678 nm band was used to derive *FLH*(678 nm) for the same data sets following the MODIS approach (i.e., the baseline was formed using bands locating at 667 and 748 nm [Letelier and Abbott, 1996], the resulting *FLH*(678 nm) showed a much lower correlation with *Chl* for Liaodong Bay, where nonphytoplankton particulate materials dominate (Figures 5e–5h, $r^2 < 0.055$, $p \gg 0.05$). *FLH*(678 nm) maintains a reasonable correlation with *Chl* for the three Indiana reservoirs, where phytoplankton is the dominant particulate material in the water, with $r^2 > 0.34$ and $p < 0.05$. However, *FLH*(678 nm) showed a nonlinear relationship with *Chl* for one group of data at the Indiana sites and became insensitive to *Chl* higher than ~ 30 mg/m^3 (Figure 5g), while the relationship appeared to be linear for the other group (Figure 5h). The factors affecting the relationships between *FLH* and *Chl* will be discussed further in section 4.2.

4. Discussion

4.1. Effect of the Fresnel Reflection of the Water Surface on *FLH*

For the reflectance spectra collected in Liaodong Bay, the radiance due to Fresnel reflection of the water surface, L_s , was not excluded. Substituting equation (1) into equation (5) and applying all the conditions in section 2.3.2 leads to

$$FLH(\lambda_2) = (1 - T_a) \times TF(\lambda_2) + \frac{L_s(\lambda_2)}{E_d(\lambda_2)} - \frac{L_s(\lambda_3)}{E_d(\lambda_3)}, \tag{8}$$

where $L_s(\lambda_2)/E_d(\lambda_2)$ and $L_s(\lambda_3)/E_d(\lambda_3)$ are the Fresnel reflectance of the water surface at λ_2 and λ_3 . According to Kutser et al. [2013], the Fresnel reflectance of the water surface between 350 and 900 nm is a power function. Therefore, $L_s(\lambda_2)/E_d(\lambda_2)$ and $L_s(\lambda_3)/E_d(\lambda_3)$ are close to each other because λ_2 and λ_3 are only 10 nm apart at ~ 761 nm. As a result, $L_s(\lambda_2)/E_d(\lambda_2) - L_s(\lambda_3)/E_d(\lambda_3)$ is negligible compared to the first term on the right-hand side of equation (8), and equation (8) becomes comparable to equation (7). In other words, the inclusion of the Fresnel reflection in the surface reflectance has a negligible impact on FLH at ~ 761 nm. The relatively flat spectrum outside the spectral peak at ~ 761 nm, shown in the insets of Figure 2, confirmed this assumption. Therefore, the reflectance spectra collected in Liaodong Bay were treated as R_{rs} for the purpose of computing $FLH(761 \text{ nm})$.

4.2. Factors Influencing the Relationships Between FLH and Chl

The results shown in Figure 5 indicate that the relationship between $FLH(761 \text{ nm})$ and Chl varied for different field campaigns. To understand the influencing factors, the biological-physical-optical mechanism of detected chlorophyll fluorescence on R_{rs} is explained below. Similar to the expression of SICF at ~ 685 nm by Maritorena et al. [2000] and Huot et al. [2005], the radiance due to local SICF (assuming no transmitted radiance from other depths) at 761 nm at depth z , $L_f(z, 761)$, can be expressed by equation (9):

$$L_f(z, 761) = \frac{\varphi Q_a(761) \int_{400}^{700} Chl(z) a_{ph}^*(\lambda) E_o(z, \lambda) d\lambda}{4\pi}, \tag{9}$$

where φ is the efficiency of Chl fluorescence at an emission wavelength of 761 nm, $Q_a(761)$ is the fraction of the emitted radiance at 761 nm that is not reabsorbed by phytoplankton cells, $a_{ph}^*(\lambda)$ is the chlorophyll a specific absorption coefficient, and $E_o(z, \lambda)$ is the total scalar irradiance at depth z .

The total above-surface radiance due to SICF, $L_f(0^+, 761)$, is a function of $L_f(z, 761)$:

$$L_f(0^+, 761) = \frac{t}{n^2} \int_0^\infty L_f(z, 761) \exp[-K_{Lu}(761)z] dz, \tag{10}$$

where $K_{Lu}(761)$ is the diffuse attenuation coefficient of upwelling radiance at 761 nm and 0^+ indicates the above-water surface.

The incident light mostly travels toward a downward direction, so E_o is assumed to approach E_d , especially in the blue and green spectral bands [Morel and Gentili, 2004], where the primary source photons of SICF are located:

$$E_o(z, \lambda) \approx E_d(z, \lambda) = t E_d(0^+, \lambda) \exp[-K_d(\lambda)z], \tag{11}$$

where $K_d(\lambda)$ is the diffuse attenuation coefficients for E_d and is also assumed to be depth independent within the top shallow layer.

Substituting equations (10) and (11) into equation (7), we can derive

$$FLH(761 \text{ nm}) \approx (1 - T_a) \frac{L_f(0^+, 761)}{E_d(0^+, 761)} \propto Chl \varphi (1 - T_a) \int_{400}^{700} a_{ph}^*(\lambda) \frac{E_d(0^+, \lambda)}{E_d(0^+, 761)} \frac{1}{K_d(\lambda) + K_{Lu}(761)} d\lambda, \tag{12}$$

with the assumption of homogenous Chl within the top layer of the water column. Such an assumption is reasonable because of the high absorption of water molecules at 761 nm unless a thin layer of phytoplankton scum is formed under blooming conditions.

Equation (12) implies that the influencing factors of the relationships between $FLH(761\text{ nm})$ and Chl may include variations in T_a , φ , $a_{ph}^*(\lambda)$, $K_d(\lambda)$, E_d , and $K_{Lu}(761)$. E_d may not be a major factor due to normalization to $E_d(0^+, 761)$, which minimizes the effects of changing illumination conditions above the water surface. $K_{Lu}(761)$ is not a major factor either due to the dominant absorption by water molecules at 761 nm, unless in rare cases where the particulate backscattering coefficient is comparable to water absorption. Among the remaining factors, T_a may have regional variability due to different atmospheric compositions, and this may partly explain why $FLH(761\text{ nm})$ has a different relationship with Chl in Liaodong Bay as compared to the Indiana reservoirs (Figure 4). φ and a_{ph}^* may vary with diurnal and seasonal changes, phytoplankton genera/species, light history, photoacclimation, and photophysiology, which subsequently leads to variations in FLH seen in Figures 5c and 5d. The data shown in Figures 5c and 5d were collected in repeated field campaigns in the three Indiana reservoirs from April to October, and it was found that $FLH(761\text{ nm})$ and Chl show different relationships for samples collected at different times of a day within the same field campaign and for samples collected at different seasons at the same site. The last factor, K_d , is not available for our data sets. Alternatively, the SPM can be an indicator of K_d [Kratzer *et al.*, 2003], although the absorption of dissolved matter should also be considered. The SPM concentrations were 87–315 g/m^3 (mean = 188.82 g/m^3) for Liaodong Bay in 2006 and 194–941 g/m^3 (mean = 530.6 g/m^3) for Liaodong Bay in 2007, 5.17–36.17 g/m^3 (mean = 15.32 g/m^3) for group 3 in Indiana, and 5.83–18.33 g/m^3 (mean = 9.77 g/m^3 after excluding only two points with $SPM > 30\text{ g/m}^3$) for group 4 in Indiana (see Table 1). The four groups can be generally separated from each other by the SPM (or the SPM -related K_d), although a small overlap of SPM between groups of the same study area could be found.

These factors may also be used to explain the current MODIS and MERIS FLH algorithms using the SICF at $\sim 685\text{ nm}$. For example, while MODIS $FLH(678\text{ nm})$ has been widely used to monitor phytoplankton blooms in sediment-poor waters rich in colored dissolved organic matter [Hu *et al.*, 2005], Gilerson *et al.* [2007] found that the $FLH(678\text{ nm})$ signal was sensitive to sediment perturbation, although the $FLH(761\text{ nm})$ signal does not appear to suffer as much as the $FLH(678\text{ nm})$ signal as a result of sediment perturbations, which can be clearly observed by comparing the results of Liaodong Bay shown in Figures 5a, 5b, 5e, and 5f. The less influence of SPM on $FLH(761\text{ nm})$ than on $FLH(678\text{ nm})$ is partially because of the spectral proximity of the bands (spanning only 16 nm) used in the formulation of $FLH(761\text{ nm})$, which negates the influence of SPM , while formation of FLH around 685 nm uses bands spanning more than 45 nm. The failure of $FLH(678\text{ nm})$ in explaining the Chl in high SPM water bodies can be additionally explained by equation (12) when applied to SICF at $\sim 678\text{ nm}$ instead of $\sim 761\text{ nm}$, which is primarily due to the variations in $K_d(\lambda)$. The influence of nonalgal material (i.e., SPM) on $FLH(678\text{ nm})$ has also been discussed by Gilerson *et al.* [2007] and McKee *et al.* [2007]. They found that increasing the mineral particulate matter, and therefore the $K_d(\lambda)$, would introduce significant uncertainties in FLH at $\sim 685\text{ nm}$ and suggested that additional caution is required to use the satellite FLH product at $\sim 685\text{ nm}$ when the SPM is high as nonalgal material will also compete with phytoplankton for photons to reduce the strength of fluorescence signal even for same Chl (see equation (12)).

The results from the Indiana reservoirs suggest additional interesting features. $FLH(678\text{ nm})$ exhibited different relationships with Chl for the two groups of the Indiana data set; i.e., one group (seven field campaigns) with a negative and nonlinear relationship and the other with a positive and linear relationship for the remaining three field campaigns. In particular, $FLH(678\text{ nm})$ becomes insensitive to $Chl > 30\text{ mg/m}^3$ (Figure 5g), which is due to the absorption of chlorophyll *a* around 670 nm and possibly lack of fluorescence from cyanobacteria [Matthews *et al.*, 2012]. The negative correlation between FLH at $\sim 678\text{ nm}$ and Chl is commonly observed for cyanobacteria-dominant water bodies because cyanobacteria fluoresce weakly due to the arrangement of pigments in their light harvesting complexes [Palmer *et al.*, 2015a]. Additional confirmation comes from the $FLH(681\text{ nm})$ data using bands at 665, 681, and 709 nm (analogy to bands 7, 8, and 9 of MERIS). The $FLH(681\text{ nm})$ values for $Chl > 10\text{ mg/m}^3$ are negative for group 3 (not shown), which is a widely observed feature of cyanobacteria [Palmer *et al.*, 2015b, and references therein]. This is expected because all three Indiana reservoirs have been facing serious cyanobacterial bloom problems. For the additional three field campaigns shown in Figure 5h, a weak positive correlation begins to appear, which might suggest weaker dominance of cyanobacteria in group 4 (assumption made in conjunction with observations in literatures). The comparison between Figures 5c and 5d may suggest that cyanobacteria has lower quantum efficiency of fluorescence than other phytoplankton species as the slope between $FLH(761\text{ nm})$ and Chl is 1 order magnitude lower in cyanobacteria-dominant waters (Figure 5c) than noncyanobacteria-

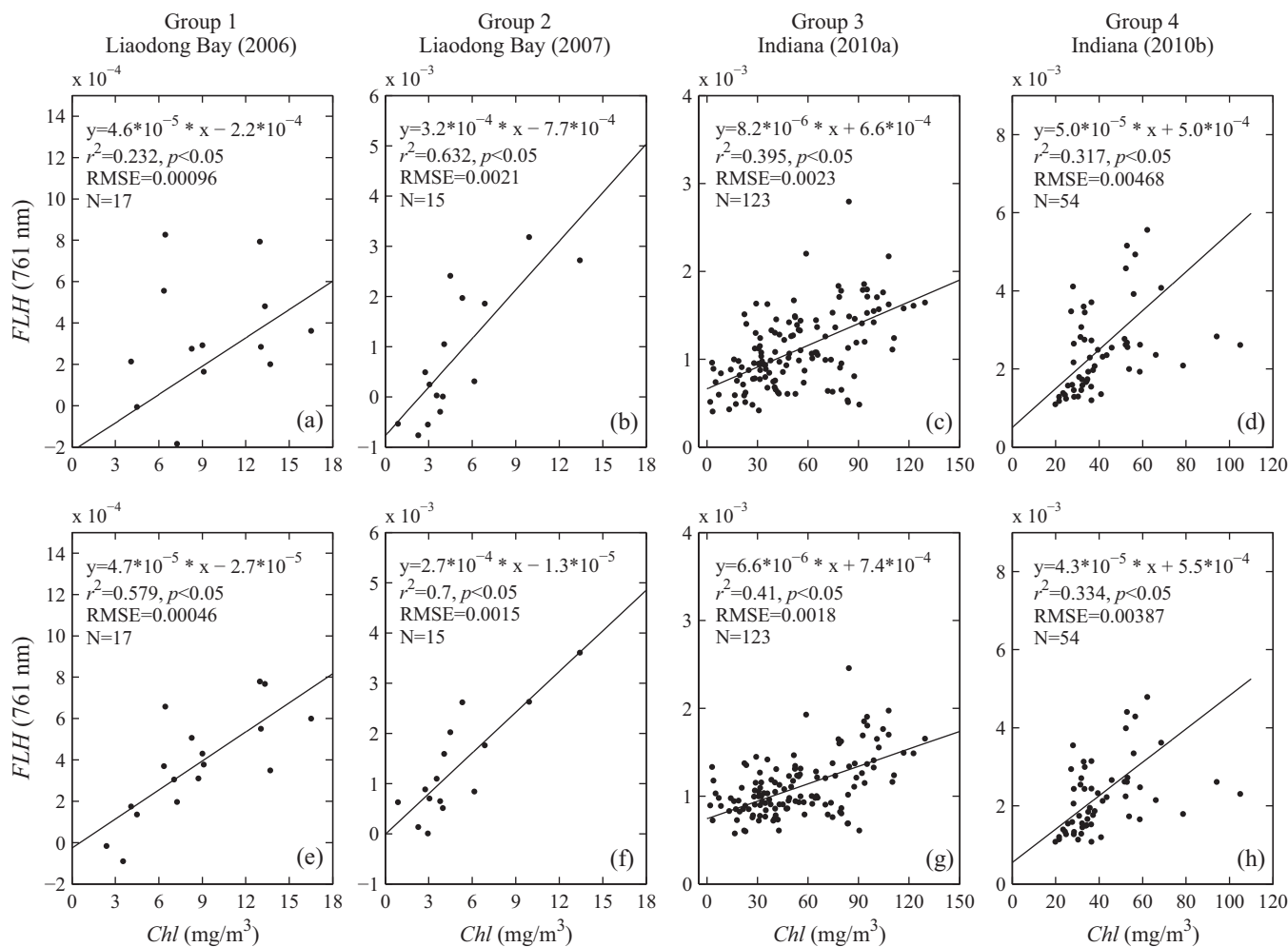


Figure 6. The relationships between $FLH(761\text{ nm})$ and Chl based on the aggregated (top row) 10 nm and (bottom row) 5 nm resolution reflectance spectra. The same groupings as in Figures 3 and 5 were used, and the same regression criteria as in Figures 5a–5d were used. The three bands used in computing $FLH(761\text{ nm})$ are centered at $\sim 750\text{ nm}$ (745–755 nm), 760 nm (755–765 nm), and 770 nm (765–775 nm) for the 10 nm resolution spectra and at $\sim 757\text{ nm}$ (755–760 nm), 762 nm (760–765 nm), and 767 nm (765–770 nm) for the 5 nm resolution spectra.

dominant waters (Figure 5d). It is well known for fluorescence at shorter wavelength of $\sim 685\text{ nm}$ where cyanobacteria fluoresce much less compared to other phytoplankton species [Yentsch and Phinney, 1985a,b]. Campbell *et al.* [1998] also suggested that cyanobacteria possess most chlorophyll in photosystem I, the main photoreaction center that produces fluorescence in the near-infrared spectral region. Thus, these results show the potentials of combining $FLH(761\text{ nm})$ and $FLH(\sim 685\text{ nm})$ to discriminate cyanobacteria-dominant waters from others, although more data need to be analyzed with more conclusive findings.

The comparison between FLH at $\sim 761\text{ nm}$ (this study) and FLH at $\sim 685\text{ nm}$ suggests that $FLH(761\text{ nm})$ is generally less affected by SPM and the phytoplankton composition (e.g., cyanobacteria). $FLH(761\text{ nm})$ always exhibited a positively linear relationship with Chl for the entire Chl range. Regardless of the potential influence of SPM , $FLH(761\text{ nm})$ shows more potential than $FLH(\sim 685\text{ nm})$ for applications in the turbid and productive coastal and inland waters if high-quality hyperspectral surface reflectance data is available. In particular, the signal of cyanobacterial fluorescence may also be detected in the spectral region around 761 nm, which could provide an alternative tool to study cyanobacterial bloom intensity. Because the relationships between $FLH(761\text{ nm})$ and Chl are affected by variations in T_{sr} , φ , a_{ph}^* , and K_d , which may change in both space and time, further efforts are required to establish a relationship to quantify Chl from $FLH(761\text{ nm})$. However, it may be challenging to establish a Chl algorithm based on $FLH(761\text{ nm})$ for large spatial scale due to high variations in these influencing factors.

4.3. Implications for Satellite Remote Sensing

The above analysis was purely based on field-measured hyperspectral data at 1 nm increments. Currently there is no hyperspectral ocean color sensor in space with such a high spectral resolution. In future, there may be hyperspectral satellite sensors such as PACE, Geo-CAPE, HypSPIRI, FLEX, or EnMAP with 5–10 nm continuous bands. Whether these bands can resolve the small *FLH* peak at ~761 nm remains a question. To answer this question, the 1 nm resolution reflectance spectra were aggregated to 10 and 5 nm resolutions, assuming a Gaussian spectral response function with Full-Width-Half-Maximum (FWHM) to be 10 and 5 nm, respectively. The aggregated 10 and 5 nm resolution spectra were then used to compute the *FLH*(761 nm) using the same methods as described in section 2.3.2.

The relationships between *FLH*(761 nm) and *Chl* using the 10 and 5 nm resolution spectra are shown in Figure 6. When the same regression approaches and criteria in Figures 5a–5d were used, the 10 nm resolution data could not achieve the same accuracy of 1 nm resolution data, as shown in Figures 5a–5d. In particular, the relationship between *FLH*(761 nm) and *Chl* for Liaodong Bay (2006) was substantially degraded, although only slight degradation was observed for the other three groups. In contrast, the 5 nm resolution data appear to be adequate in achieving similar or even higher accuracy than the 1 nm resolution data. Therefore, the SICF feature at ~761 nm of natural turbid and productive waters may be captured by future hyperspectral ocean color satellite sensors with a 5 nm spectral resolution.

However, the findings above are based on the assumptions that atmospheric correction of satellite measurements is error free. In reality, this is not the case. Although spectrally flat atmospheric correction errors [Hu *et al.*, 2013] may not influence band-subtraction algorithms, such as the *FLH* algorithm or the color index (CI) algorithm [Hu *et al.*, 2012a], the influence of variable aerosol height (e.g., troposphere aerosols and cirrus clouds) on the total at-sensor signal around the wavelength of 761 nm cannot be neglected [Ding and Gordon, 1995]. Indeed, the SeaWiFS 765 nm band, which encompasses the 761 nm absorption line, was used to estimate aerosol height [Dubuisson *et al.*, 2009]. To fully utilize the *FLH*(761 nm) algorithm, such effects must be fully understood and corrected for future satellite sensors in order to assure error-free R_{rs} retrievals or at least spectrally linear R_{rs} errors in the retrievals. For the same reason, the satellite sensors must have enough sensitivity (or signal-to-noise ratio, SNR) to quantify the small reflectance peak around 761 nm (often between $10^{-4} - 10^{-3} \text{ sr}^{-1}$, Figure 5). For reference, the SNR of the MODIS 748-nm band is about 1000:1 at typical radiance input of $0.75 \text{ mW cm}^{-2} \mu\text{m}^{-1} \text{ sr}^{-1}$ [Hu *et al.*, 2012b], leading to reflectance errors in the order of $<10^{-5} \text{ sr}^{-1}$ and thus sufficient for this purpose.

5. Conclusions

The SICF exhibits two dominant spectral peaks around 685 and 740 nm. The SICF at 685 nm has been widely applied to studies of natural waters. The SICF at ~761 nm has also been used to study terrestrial vegetation due to the fill-in effect on the Telluric line caused by oxygen absorption. However, the SICF at ~761 nm has never been applied to natural waters to study algal blooms. Instead, the small reflectance peak around 761 nm measured from natural waters has often been treated as measurement artifacts. In this study, we have demonstrated that such a peak from natural waters (Liaodong Bay in China and three Indiana reservoirs in the USA) was also caused by SICF. This finding is supported by several lines of evidence including a first-order derivative analysis of the reflectance spectra and a correlation analysis between *FLH*(761 nm) and *Chl*. The theoretical basis of the correlation between *FLH*(761 nm) and *Chl* is the same as that between *FLH*(678 nm) and *Chl*, while the factors influencing such relationships were also the same. However, the former relationship appears to be less affected by *SPM* and phytoplankton composition, making *FLH*(761 nm) a potentially better spectral index for estimating *Chl* of extremely turbid coastal and inland waters where *SPM* may be high, and for discriminating cyanobacteria-dominant waters from others. Yet developing such an index still requires further data collection and more in-depth analysis.

The relationship between *FLH*(761 nm) and *Chl* does not degrade when the 1 nm resolution reflectance data are aggregated to a 5 nm resolution, suggesting that the *FLH*(761 nm) signal might be captured by future satellite sensors with 5 nm resolution continuous bands provided that errors from atmospheric correction are negligible or spectrally linear. However, given the changing optical composition and variable fluorescence efficiency, it may not be able to establish a universal, region-independent *Chl* algorithm using

FLH(761 nm). Further research is required to confirm and refine such relationships for various water types under different conditions, and their sensitivity to atmospheric correction errors due to variable aerosol heights also needs to be addressed before an application can be developed to use satellite data.

Acknowledgments

This work was supported by the National Natural Science Foundation of China (Grant No. 41371014), the Open Research Fund of State Key Laboratory of Satellite Ocean Environment Dynamics (Second Institute of Oceanography, SOA) (SOED1608), and the Open Research Fund of Key Laboratory of Digital Earth Science, Institute of Remote Sensing and Digital Earth, Chinese Academy of Sciences (No. 2013LDE005). The authors thank CEES at IUPUI for assisting in field sampling as well as students and postdocs in Lin Li's laboratory for analyzing water samples collected in three Indiana reservoirs in 2010 and ESS1 at NJU for collecting data from Liaodong Bay in 2006 and 2007. We also thank the National data sharing infrastructure of Earth System Science for providing some of geographical data (<http://www.geodata.cn/>). We are grateful to Dr. Mark William Matthews and the other anonymous reviewer who provided valuable comments to help improve this paper.

References

- Campbell, D., V. Hurry, A. K. Clarke, P. Gustafsson, and G. Öquist (1998), Chlorophyll fluorescence analysis of cyanobacterial photosynthesis and acclimation, *Microbiol. Mol. Biol. Rev.*, *62*(3), 667–683.
- Damm, A., A. Erler, W. Hillen, M. Meroni, M. E. Schaepman, W. Verhoef, and U. Rascher (2011), Modeling the impact of spectral sensor configurations on the FLD retrieval accuracy of sun-induced chlorophyll fluorescence, *Remote Sens. Environ.*, *115*(8), 1882–1892, doi:10.1016/j.rse.2011.03.011.
- Ding, K., and H. R. Gordon (1995), Analysis of the influence of O₂ A-band absorption on atmospheric correction of ocean-color imagery, *Appl. Opt.*, *34*, 2068–2080, doi:10.1364/AO.34.002068.
- Dubuisson, P., R. Frouin, D. Dessailly, L. Duforêt, J. Léon, K. Voss, and D. Antoine (2009), Estimating the altitude of aerosol plumes over the ocean from reflectance ratio measurements in the O₂ A-band, *Remote Sens. Environ.*, *113*, 1899–1911, doi:10.1016/j.rse.2009.04.018.
- Gilerson, A., J. Zhou, S. Hlaing, I. Ioannou, J. F. Schalles, B. Gross, F. Moshary, and S. Ahmed (2007), Fluorescence component in the reflectance spectra from coastal waters. Dependence on water composition, *Opt. Express*, *15*, 15,702–15,721, doi:10.1364/OE.15.015702.
- Gitelson, A. A. (1992), The peak near 700 nm on radiance spectra of algae and water: Relationships of its magnitude and position with chlorophyll concentration, *Int. J. Remote Sens.*, *13*(17), 3367–3373, doi:10.1080/01431169208904125.
- Gitelson, A. A., J. F. Schalles, and C. M. Hladik (2007), Remote chlorophyll-a retrieval in turbid, productive estuaries: Chesapeake Bay case study, *Remote Sens. Environ.*, *109*(4), 464–472, doi:10.1016/j.rse.2007.01.016.
- Gordon, H. R. (1974), Spectral variations in the volume scattering function at large angles in natural waters, *J. Opt. Soc. Am.*, *64*(6), 773–775, doi:10.1364/JOSA.64.000773.
- Gordon, H. R. (1979), Diffuse reflectance of the ocean: The theory of its augmentation by chlorophyll a fluorescence at 685nm, *Appl. Opt.*, *18*(8), 1161–1166, doi:10.1364/AO.18.001161.
- Gordon, H. R., O. B. Brown, R. H. Evans, J. W. Brown, R. C. Smith, K. S. Baker, and D. K. Clark (1988), A semianalytic radiance model of ocean color, *J. Geophys. Res.*, *93*, 10,909–10,924, doi:10.1029/JD093iD09p10909.
- Hu, C., and K. J. Voss (1998), Measurement of solar-stimulated fluorescence in natural waters, *Limnol. Oceanogr.*, *43*, 1198–1206, doi:10.4319/lo.1998.43.6.1198.
- Hu, C., F. E. Muller-Karger, C. Taylor, K. L. Carder, C. Kelble, E. Johns, and C. Heil (2005), Red tide detection and tracing using MODIS fluorescence data: A regional example in SW Florida coastal waters, *Remote Sens. Environ.*, *97*, 311–321, doi:10.1016/j.rse.2005.05.013.
- Hu, C., Z. Lee, and B. Franz (2012a), Chlorophyll algorithms for oligotrophic oceans: A novel approach based on three-band reflectance difference, *J. Geophys. Res.*, *117*, C01011, doi:10.1029/2011JC007395.
- Hu, C., L. Feng, Z. Lee, C. O. Davis, A. Mannino, C. R. McClain, and B. A. Franz (2012b), Dynamic range and sensitivity requirements of satellite ocean color sensors: learning from the past, *Appl. Opt.*, *51*(25), 6045–6062, doi:10.1364/AO.51.006045.
- Hu, C., L. Feng, and Z. Lee (2013), Uncertainties of SeaWiFS and MODIS remote sensing reflectance: Implications from clear water measurements, *Remote Sens. Environ.*, *133*, 163–182, doi:10.1016/j.rse.2013.02.012.
- Huot, Y., C. A. Brown, and J. J. Cullen (2005), New algorithms for MODIS sun-induced chlorophyll fluorescence and a comparison with present data products, *Limnol. Oceanogr. Methods*, *3*(2), 108–130, doi:10.4319/lom.2005.3.108.
- Krause, G. H., and E. Weis (1991), Chlorophyll fluorescence and photosynthesis: The basics, *Annu. Rev. Plant Physiol. Plant Mol. Biol.*, *42*, 313–349, doi:10.1146/annurev.pp.42.060191.001525.
- Kratzer, S., B. Håkansson, and C. Sahlin (2003), Assessing Secchi and photic zone depth in the Baltic Sea from satellite data, *Ambio*, *32*(8), 577–585, doi:10.1579/0044-7447-32.8.577.
- Kutser, T., E. Vahtmäe, B. Paavel, and T. Kauer (2013), Removing glint effects from field radiometry data measured in optically complex coastal and inland waters, *Remote Sens. Environ.*, *133*(15), 85–89, doi:10.1016/j.rse.2013.02.011.
- Lee, Z., K. Carder, R. Arnone, and M. He (2007), Determination of primary spectral bands for remote sensing of aquatic environments, *Sensors*, *7*(12), 3428–3441, doi:10.3390/s7123428.
- Letelier, R. M., and M. R. Abbott (1996), An analysis of chlorophyll fluorescence algorithms for the Moderate Resolution Imaging Spectrometer (MODIS), *Remote Sens. Environ.*, *58*(2), 215–223, doi:10.1016/j.rse.2013.02.011.
- Li, L., L. Li, K. Song, Y. Li, L. P. Tedesco, K. Shi, and Z. Li (2013), An inversion model for deriving inherent optical properties of inland waters: Establishment, validation and application, *Remote Sens. Environ.*, *135*, 150–166, doi:10.1016/j.rse.2013.03.031.
- Li, L., L. Li, and K. Song (2015), Remote sensing of freshwater cyanobacteria: An extended IOP Inversion Model of Inland Waters (IIMIW) for partitioning absorption coefficient and estimating phycocyanin, *Remote Sens. Environ.*, *157*, 9–23, doi:10.1016/j.rse.2014.06.009.
- Maritorena, S., A. Morel, and B. Gentili (2000), Determination of the fluorescence quantum yield by oceanic phytoplankton in their natural habitat, *Appl. Opt.*, *39*, 6725–6737, doi:10.1364/AO.39.006725.
- Matthews, M. W., S. Bernard, and L. Robertson (2012), An algorithm for detecting trophic status (chlorophyll-a), cyanobacterial-dominance, surface scums and floating vegetation in inland and coastal waters, *Remote Sens. Environ.*, *124*, 637–652, doi:10.1016/j.rse.2012.05.032.
- McKee, D., A. Cunningham, D. Wright, and L. Hay (2007), Potential impacts of nonalgal materials on water-leaving Sun induced chlorophyll fluorescence signals in coastal waters, *Appl. Opt.*, *46*(31), 7720–7729, doi:10.1364/AO.46.007720.
- Meroni, M., and R. Colombo (2006), Leaf level detection of solar induced chlorophyll fluorescence by means of a subnanometer resolution spectroradiometer, *Remote Sens. Environ.*, *103*(4), 438–448, doi:10.1016/j.rse.2006.03.016.
- Meroni, M., M. Rossini, L. Guanter, L. Alonso, U. Rascher, R. Colombo, and J. Moremo (2009), Remote sensing of solar-induced chlorophyll fluorescence: Review of methods and applications, *Remote Sens. Environ.*, *113*(10), 2037–2051, doi:10.1016/j.rse.2009.05.003.
- Mobley, C. D. (1999), Estimation of the remote-sensing reflectance from above-surface measurements, *Appl. Opt.*, *38*, 7442–7445, doi:10.1364/AO.38.007442.
- Morel, A., and B. Gentili (2004), Radiation transport within oceanic (case 1) water, *J. Geophys. Res.*, *109*, C06008, doi:10.1029/2003JC002259.
- Moya, I., L. Camenen, S. Evain, Y. Goulas, Z. G. Cerovic, G. Latouche, J. Flexas, and A. Ounis (2004), A new instrument for passive remote sensing: 1. Measurements of sunlight-induced chlorophyll fluorescence, *Remote Sens. Environ.*, *91*(2), 186–197, doi:10.1016/j.rse.2004.02.012.

- Neville, R. A., and J. F. R. Gower (1977), Passive remote sensing of phytoplankton via chlorophyll fluorescence, *J. Geophys. Res.*, *82*, 3487–3493, doi:10.1029/JC082i024p03487.
- Palmer, S. C. J., et al. (2015a), Validation of Envisat MERIS algorithms for chlorophyll retrieval in a large, turbid and optically-complex shallow lake, *Remote Sens. Environ.*, *157*, 158–169, doi:10.1016/j.rse.2014.07.024.
- Palmer, S. C. J., D. Odermatt, P. D. Hunter, C. Brockmann, M. Presing, H. Balzter, and V. R. Tóth (2015b), Satellite remote sensing of phytoplankton phenology in Lake Balaton using 10 years of MERIS observations, *Remote Sens. Environ.*, *158*(1), 441–452, doi:10.1016/j.rse.2014.11.021.
- Ritchie, R. J. (2008), Universal chlorophyll equations for estimating chlorophylls a, b, c, and d and total chlorophylls in natural assemblages of photosynthetic organisms using acetone, methanol, or ethanol solvents, *Photosynthetica*, *46*(1), 115–126, doi:10.1007/s11099-008-0019-7.
- Tyler, J. E., and R. C. Smith (1970), *Measurements of Spectral Irradiance Under Water*, Gordon and Breach, N. Y.
- Yentsch, C. S., and D. A. Phinney (1985a), Spectral fluorescence: An ataxonomic tool for studying the structure of phytoplankton populations, *J. Plankton Res.*, *7*(5), 617–632, doi:10.1093/plankt/7.5.617.
- Yentsch, C. S., and D. A. Phinney (1985b), Fluorescence spectral signatures of marine phytoplankton, in *Mapping Strategies in Chemical Oceanography, Adv. Chem. Ser.*, vol. 209, edited by A. Zirino, pp. 259–274, Am. Chem. Soc., Washington, D. C.
- Zarco-Tejada, P. J., J. A. J. Berni, L. Suárez, G. Sepulcre-Cantó, F. Morales, and J. R. Miller (2009), Imaging chlorophyll fluorescence with an airborne narrow-band multispectral camera for vegetation stress detection, *Remote Sens. Environ.*, *113*(6), 1262–1275, doi:10.1016/j.rse.2009.02.016.